# MIXING AND UNMIXEDNESS IN PLASMA JETS 1: NEAR-FIELD ANALYSIS

Olusegun J. Ilegbusi
Department of Mechanical Engineering
Northeastern University
Boston, MA 02115

## SUMMARY

The flow characteristics in the near-field of a plasma jet are simulated with a two-fluid model. This model accounts for both gradient-diffusion mixing and uni-directional sifting motion resulting from pressure-gradient-body-force imbalance. This latter mechanism is believed to be responsible for the umixedness observed in plasma jets. The unmixedness is considered to be essentially a Rayleigh-Taylor kind instability. Transport equations are solved for the individual plasma and ambient gas velocities, temperatures and volume fractions. Empirical relations are employed for the interface transfers of mass, momentum and heat. The empirical coefficients are first established by comparison of predictions with available experimental data for shear flows. The model is then applied to an Argon plasma jet ejecting into stagnant air. The predicted results show the significant build-up of unmixed air within the plasma gas, even relatively far downstream of the torch. By adjusting the inlet condition, the model adequately reproduces the experimental data.

## INTRODUCTION

Plasma jets have important applications in materials processing, some of which include spray deposition, melting and refining, heat treatment and materials synthesis. In a typical reactor, the hot plasma stream entrains a surrounding gas and the resulting heat and mass transfer and the condition of operation of the torch, determines to a large extent, the performance of the unit. The entrainment may prevent uniform mixing and produce regions of unmixed hot/cold gases and non-uniform deposits as a result of insufficient melting of deposit in cold regions. This phenomenon may also affect chemical reaction rate in plasma systems for NOx reduction in exhaust gases.

The study of plasma phenomena is often conveniently divided into three parts namely, the plasma torch, the plasma jet and analysis of the particles carried in the jet. The present work concerns processes occuring in the near-field of the plasma jet i.e. just downstream of the torch.

The early modeling approaches on plasma jets were based on the solution of momentum integral equations (refs. 1 and 2), and on highly simplified boundary layer equations (refs. 3 and 4). These techniques, while providing useful insights into the gross behavior of plasma jets, were inadequate due to their inherent approximations. A fully elliptic approach was employed later by several workers (refs. 5-10), with varying degrees of success. Such works ranged in complexity, depending on the assumptions made for the inlet conditions, property variation and treatment of the surrounding gas. They have shown that:

(i)   the velocity and temperature profiles within the reactor are strongly dependent on the torch exit conditions,

(ii)  plasma jets operating in a fully laminar regime could be adequately modeled by existing methodologies, and,

(iii) plasma jets operating in a fully turbulent regime could not be adequately simulated with existing conventional turbulence models. Specifically, such models could not account for the inherent non-isotropic, intermittent nature of the turbulence field.

Recent studies (refs. 11 to 14) have shown that contrary to earlier beliefs, the flow emanating from most standard torches is highly transitional over most of the domain of the reactor, and mixing of the plasma jet with the cold surrounding gas is dominated by large scale coherent structures. Clearly, prediction methods which assume uniform properties resulting from small-scale mixing processes (such as the popular k-ε model) will be highly unreliable. Specifically, the phenomenon of unmixedness cannot be predicted by conventional turbulence models.

The objective of this study is to employ a two-fluid model (refs. 15 to 17) to predict the degree of mixing and unmixeness in the near-field region of a typical plasma reactor. The two-fluid idea has been employed in various forms by many authors (refs. 18 to 23). The present model has however refined those ideas by employing the mathematical techniques that have been developed for two-phase flows. The model requires solution of conservation equations of two sets of velocities and temperatures, and also of the volume fractions. It also requires mathematical representation of each of the processes of interaction between the the two fluids such as momentum and heat exchange and entrainment of one fluid by the other. Additional relations are required to express the transport of fluid fragments due to relative motion of the two fluids. The model has been applied successfully to boundary layers and internal flows in earlier publications (refs. 16,17, and 24 to 26). In the present paper, the main features of the model are presented and applied to flow in a plasma reactor.

A parabolic solution technique has been employed to ensure adequate grid resolution and numerical accuracy of the results. It should be mentioned that while a fully elliptic model does not suffer from the approximations to the governing equations imposed by the parabolic scheme, it requires calculation of the whole domain of the reactor, including the stagnant region outside the jet, where little or no property variations occur. Indeed, ellipticity (or flow recirculation) is confined essentially to this outer ambient region and its neglect is not expected to have significant effect on the results within the plasma jet. The present parabolic approach allows us to concentrate the computational grid within the jet region of interest.

The paper is divided into five main sections of which this introduction is the first. In the following section, we describe a brief mathematical formulation of the two fluids model. Section 3 provided details of the computational method employed to solve the governing transport equations. The results are presented and discussed in section 4. Finally, section 5 contains the concluding remarks.

## MATHEMATICAL FORMULATION

### The Two-Fluid Idea

We propose that the observed mixing and unmixedness in plasma jets could be explained to a significant extent, by a "sifting" phenomenon, in which fragments of fluid subjected to larger body forces move through those subjected to smaller body forces in a pressure gradient field. This phenomenon is similar to the Rayleigh-Taylor kind instabilities.

The body forces are here due to the large thermal field gradient between the plasma gas and the ambient air. This sifting motion is essentially one-dimensional. Conventional turbulence models such as the k-ε model have terms to express gradient diffusion fluxes or shear stresses which in the present situation represents only an additional mechanism responsible for mixing. These models have no terms to account for the often counter-gradient unmixing phenomenon.

The sifting phenomenon can be represented mathematically by considering space as containing a mixture of fragments of two distinct fluids, separated by sharp (but flexible and permeable) boundaries on which surface tension are inactive. In effect, while conventional models are concerned with time-averaged properties of fluid, the present two-fluid model focuses on averages of conditioned quantities. At any location, we thus have two average densities, two velocities in each coordinate direction and two temperatures.

The most general means of distinguishing between the two fluids is to suppose that fluid 1 has a greater time-averaged velocity $v_1$, and fluid 2 a lesser one, $v_2$, in the body-force direction. This definition allows a direct qualitative physical relationship to Prandtl's mixing-length theory (ref. 19). Fortunately, in the present situation, this implies that fluid 1 is the hot plasma gas while fluid 2 is the cold ambient air surrounding the jet. The two fluids are assumed to share space in proportion to their existence probabilities or volume fractions, $r_1$ and $r_2$, such that:

$$r_1 + r_2 = 1.0 \tag{1}$$

In this and subsequent equations, subscript 1 refers to the plasma gas (Argon) while subscript 2 refers to the ambient air (or Nitrogen).

Transport equations are required for each fluid, with empirical relations to express the entrainment and transfer of momentum and heat at the interface.

### General Conservation Equation (Fluid i)

In light of the above, the set of partial differential conservation equations governing the transport of a generic flow variable $\phi$ for fluid i (i=1 for plasma gas, i=2 for ambient air) in plasma jet can be represented as:

$$\frac{\partial}{\partial t}(r_i \rho_i \phi_i) + \nabla \cdot (r_i \rho_i U_i \phi_i - \Gamma_i \nabla \phi_i) = S_i + S_i^* \tag{2}$$

in which,

$\phi$ ≡ dependent variable (= 1 for continuity)
r ≡ volume fraction
Γ ≡ relevant transport property (exchange coefficient, representing effect of diffusion within one fluid)
U ≡ velocity vector
S ≡ intra-fluid source terms (e.g. pressure gradient and buoyancy forces)
$S^*$ ≡ inter-fluid source terms (friction, entrainment, heat conduction at interface)

The dependent variables and the associated definitions of Γ, S and S* are presented in Table 1. Details of the derivation of these expressions are contained in refs. 16 and 17. The

set of values of the model constants employed in the analysis is presented in Table 2. These values have been established in earlier work on boundary layers and free shear flows (refs. 16, 17 and 24). In Table 1, subscripts i and j refer to the two fluids, E represents the entrainment rate, F is the interface friction and Q is the heat conduction at the interface. Auxiliary relations are employed to express these terms as follows:

Entrainment Rate: We assume that the rate of entrainment is proportional to the relative velocity of the two fluids and to the surface area of the fragment. Assuming j represents the fragment phase, the entrainment rate per unit volume can thus be expressed as:

$$E_{ij} = c_m \rho_i r_i r_j (r_j - 0.5) |\Delta U|/l \tag{3}$$

where $c_m$ is an empirical constant and $l$ is a measure of the linear scale of the fragment and characterizes the interaction processes between the two fluids, $|\Delta U|$ represents the relative velocity between the fluid and its surrounding. The term $(r_j - 0.5)$ is used to enforce symmetry and ensure generality of application of the model to free and confined flows.

Inter-Fluid Friction Forces: The friction forces per unit volume that fluid j exterts on fluid i is expressed as:

$$F_{ij} = c_f \rho_i r_i r_j (U_j - U_i) |\Delta U|/l \tag{4}$$

in which $c_f$ is an empirical constant and U represents either the cross-stream or streamwise velocity components, depending on the momentum equation of interest. Equation (4) implies that the slower-moving fluid gains momentum from the fast-moving fluid. This momentum transfer is of course in addition to that due to the mass transfer as a result of entrainment between the fluids.

Inter-Fluid Heat Transfer: The heat conduction at the interface from fluid j to fluid i is expressed in analogy to the above inter-fluid momentum flux as:

$$Q_{ij} = c_h c_p \rho_i r_i r_j (T_j - T_i) |\Delta U|/l \tag{5}$$

where $c_h$ is an empirical constant (established in ref. 24) and $c_p$ is the specific heat of the hot fluid at constant pressure. In effect, the hot fluid looses heat to the cold fluid at any spatial location.

Shear Source $S_{vi}$: By analogy to Prandtl's hypothesis, we postulate that there should be a shear-related source in the cross-stream momentum equations (for $v_1$ and $v_2$) that is proportional to the gradient of the mean streamwise velocity. This source term can be expressed as:

$$S_{vi} = c_v \rho_i |\Delta U| \left| \frac{\partial w}{\partial y} \right| \tag{6}$$

in which $c_v$ is an empirical constant and w is the mean velocity in the main flow direction. This equation implies that $v_1$ will increase and $v_2$ will decrease, whenever the two fluids are in relative motion and the main flow exhibits shear (i.e. $|\partial w/\partial y| > 0$). This term thus expresses

the well-known instability of shear layers and their tendency to break up into a succession of eddies or train of vortices which are convected downstream at the mean-flow velocity.

Length Scale $l$: While the actual entrainment process in shear flows and perhaps plasma jets may depend in detail on viscous action, evidence abounds indicating that the entrainment rate is controlled by the large-scale motion (refs. 11 and 26). We here employ the following transport equation to obtain the length scale thus:

$$\frac{\partial l}{\partial t} + \mathbf{U} \cdot \nabla l = A|\mathbf{U}| - B\,l\left(\frac{\partial v}{\partial z} + \frac{\partial w}{\partial y}\right) \tag{7}$$

in which $A$ and $B$ are constants. The first term on the right hand side expresses the growth of fragment size by entrainment and agglomeration. The second term represents the decrease of fragment size by shear distortion. The preliminary values employed for the constants are $A = 0.05$ and $B = 0.01$.


Boundary and Initial Conditions

Symmetry Plane: The physical situation considered is symmetrical about the jet axis, and so calculations are performed only over one half of the flow. A no-flux boundary condition is thus imposed at the symmetry plane.

Free stream: At the outer edge of the computational domain which is located in the ambient air stream just beyond the jet boundary, a fixed pressure condition is imposed. Thus, mass transfer or entrainment of air across this boundary is calculated from continuity. The main-stream velocities and temperatures are prescribed to equal the values in the surrounding air.

The parabolic numerical approach employed implies there is a predominant direction of flow. The nature of the governing equations is such that the downstream boundary condition is of no consequence and needs not (and indeed, should not) be prescibed.

Initial Conditions: Since the calculations must start from an inlet plane, the initial distribution of the dependent variables (velocities, temperatures, volume fractions) must be specified. At the torch exit which represents the inlet plane to the computational domain, parabolic velocity and temperature profiles are prescibed within the jet using the following relations:

$$v_1 = v_{max}\,[\,1 - (r/r_0)^2\,] \tag{8}$$

$$T_1 = T_{max}\,[\,1 - (r/r_0)^2\,] \tag{9}$$

wherein $v_{max}$(=400m/s), $T_{max}$ (=11500K) are the maximum velocity and temperature at the axis, $v_1$ and $T_1$ are the velocity and temperature of the Argon (plasma gas) respectively, $r$ is the radial coordinate and $r_0$ is the radius of the torch. The values employed for these parameters are contained in Table 3. The volume fraction of the plasma gas ($r_1$) is also specified to be unity at this location.

# COMPUTATIONAL DETAILS

Grid: A total of 40 non-uniform grids are employed in the radial direction, with about 90% located within the jet. The computational domain is allowed to expand linearly with the downstream direction in the form:

$$r_g/r_0 = a + bz \tag{10}$$

where $r_g$ is the radial extent of the grid, $r_0$ is the torch exit radius (jet radius at inlet plane), z is the streamwise distance from the inlet and $a$ and $b$ are empirical constants. The established spreading rate of axisymmetric jets is used to estimate the initial magnitudes of $a$ and $b$. The estimated values are then systematically modified until the computational grid spreads slightly faster than the jet. The values employed in the present study are $a = 1.0$ and $b = 18.50$.

Solution Procedure: The above governing differential equations are solved using the Inter-Phase Slip (IPSA) algorithm embodied in the PHOENICS computational code (ref. 27). The IPSA algorithm has been described in detail in several publications (refs. 28 to 30). This algorithm allows for shared pressure between the two fluids and employs a Partial Elimination Algorithm (PEA) to accelerate convergence of the solutions of the finite domain equations for the temperatures and velocities.

The thermodynamic and transport properties of the plasma gas (Argon) and air are obtained from the literature (refs. 31 to 33). The principal input parameters employed in the computation are presented in Table 3.

# RESULTS

## Prelimianry Application to Shear Flows

Figs. 1 shows a comparison of the mean and conditioned temperature similarity profiles with the experimental data (refs. 34 to 39), for a plane jet ejecting into stagnant environments. The corresponding results for an axisymmetric jet are presented in Fig.2. The predicted and measured shear stresses and heat fluxes are presented in Figs.3 and 4 for a plane jet and an axisymmetric jet, respectively. The predicted gross characteristics of jets are compared with the values deduced from the experimental data in Table 4.

The mean characteristics and fluxes in the above and subsequent figures are calculated from the individual fluid variables and the volume fractions using the following relations:

$$\phi = r_1\phi_1 + r_2\phi_2 \tag{11}$$

$$\overline{v\phi} = r_1 r_2 (v_1 - v_2)(\phi_1 - \phi_2) \tag{12}$$

where $\phi$ represents velocity or temperature.

These results have shown that the two-fluid model, employing the model constants presented in Table 2, can adequately predict the flow characteristics of turbulent shear flows.

312

Fig. 5 shows a schematic sketch of the calculation domain considered. The initial width of the grid is located at the torch exit, and the forward step size is progressively increased until a distance of about 8 torch diameters is reached. This ensures that predictions are restricted to the near-field region of the jet. Figs. 6 and 7 show respectively the velocity vectors and mean temperature profiles in the plasma jet. These figures clearly show the spread of the jet along the reactor, and the decay of the jet velocity and temperature downstream of the torch. The hot and fast-moving core of the plasma is clearly visible from these figures, as well as the slow, cold region near the edge of the jet.

The decay of centerline mean velocity and temperature are shown in Figs. 8 and 9. Fig. 10 shows the increase in fraction of Nitrogen (or ambient air) along the centerline while Fig. 11 presents the profiles of the volumetric entrainment rate in the jet. Clearly, there occur sharp decreases in the velocity and temperature profiles at locations corressponding to the increase in entrainment rate. Fig. 11 shows that at any axial location, the entrainment rate reaches a maximum near the edge of the jet . It should be remarked that the outer edge of Fig. 11 (as in other figures showing the complete domain) corresponds to the outer edge of the computational grid, while the edge of the jet is somewhat narrower.

Equally significant is that Fig. 10 indicates that a significant portion of the core region of the jet consists of ambient Nitrogen downstream of the torch. While subsequent mixing might allow this to decay farther downstream, this result clearly confirms the occurence of unmixed fragments of ambient fluid within the plasma.

Figs 12 and 13 show the radial profiles of predicted conditioned velocities and temperatures respectively, at a location z/D=5, downstream of the torch, D being the diameter of the torch exit. Figs. 14 and 15 show the field profiles of Argon temperature and Nitrogen (Air) temperature respectively. In Figs. 16 and 17 are presented the Argon and Nitrogen temperature profiles, respectively, at three axial locations (z/D=3, 5 and 8). These figures show that Argon temperature is generally higher than Nitrogen temperature; the difference progressively decreasing downstream as entrainment increases. At a location just downstream of the torch (z/D=3), the plasma temperature decreases rapidly due to large entrainment of Nitrogen, and then decreases towards the free stream. Fig. 16 shows that at large radial locations, the plasma temperature near the torch is smaller than that far downstream due to the spread of the jet. For instance, while location $r$ = 6mm might be located in the low temperature, ambient region at z/D=3, the same radial position would be located well within the expanding jet at z/D=8, father downstream of the torch.

In Figs. 18 and 19 are presented a comparison of the predicted temperature centerline and radial temperature profiles respectively with the experimental data (ref. 40). To obtain this fit, the inlet velocity and temperature profiles have been expressed using the following relations:

$$v = v_{max} [ 1 - (r/r_0)^3] \qquad (13)$$

$$T = T_{max} [ 1 - (r/r_0)^3] \qquad (14)$$

where $v_{max}$=600m/s and $T_{max}$ = 11500 K. This approach was taken due to lack of available data for the conditions at the torch exit. While the results appear satisfactory, the work is still very preliminary at this stage. A more detailed study of this problem will be considered in a subsequent publication. These figures however show that, with the appropriate inlet and

boundary conditions, the experimental data on jets can be well simulated by the two-fluids model.

## CONCLUSION

A two-fluid model of turbulence has been presented that accounts for unidirectional "sifting" resulting from body-force-pressure gradient imbalnace, as well as the stress induced (gradient diffusion) mechanism. The sifting mechanism is believed to be responsible for the observed unmixing in many systems including plasma reactors.

Empirical correlations are employed to represent interfluid phenomena including entrainment rate, friction and heat conduction at the interface. The model constants were established from prior work by comparison of predictions with available mean and conditional sampling data for shear layers.

The model was then applied to predict the flow characteristics in a plasma jet issuing into a stagnant ambient air in a reactor. It allows for the prediction of not only the mean velocity and temperature profiles, but also, the spatial distribution of the Argon (Plasma gas) and Nitrogen velocity and temperature, volume fractions and entrainment rate.

The results appear to be qualitatively realistic and the model appears to be a useful tool for predicting mixing and unmixedness in plasma jets. We have been able to predict the decay in flow velocity and temperature as a result of entrainment of ambient Nitrogen. There appears to be a significant concentration of Nitrogen in the core of the plasma even at relatively long distance downstream of the torch, indicating the occurence of unmixed zones. A preliminary calculation also shows that by adjusting the inlet profiles, we can successfully reproduce the experimental data for a plasma jet. Details of this work will appear in a subsequent paper.

Further work is being planned to compare predictions with more experimental data. The ultimate objective is to combine this model with a large eddy simulation scheme to predict the large structures observed experimentally, and to study the transitional flow behavior in the plasma reactor.

## REFERENCES

1. Grey, J; Sherman,M.P.; Williams, P.M.; and Frodkin, D.B.: AIAA J., vol. 4, 1966, p.986.
2. Donaldson,C.P.; and Gray, K.E.: AIAA J., vol.4, 1966, p.2017.
3. Incropera, I.P.; and Leppert, G.: Int. J. Heat Mass Transfer, vol. 10, 1967, p.1861.
4. Lee, Y.C.; and Pfender, E.: Plasma Chem. Plasma Proc., vol. 7, (1), 1987, p.1.
5. Mckelliget, J.; Szekely, J.; Vardelle, M.; and Fauchais, P.: Plasma Chem. Plasma Proc., vol. 2, 1982, p.317.
6. Dilawari, A.H.; and Szekely, J.: Int. J. Heat Mass Trans. vol. 30, (11), 1987, p.2357.
7. Dilawari, A.H.; Szekely, J.; Coudert, J.F.; and Fauchais, P.: Int. J. Heat Mass Trans., vol. 32, (1), 1989, p.35.
8. Chyou, Y.P.; and Pfender, E.: Plasma Chem. Plasma Proc., vol. 9, (2), 1989, p.291.
9. Chang, C.H.; and Pfender, E.: Plasma Chem. Plasma Proc., vol. 10, (3), 1990, p. 473.
10. Chang, C.H.; and Pfender, E.: Plasma Chem. Plasma Proc., vol. 10, (3), 1990, p. 493.
11. Pfender, E.; Finke, J.; and Spores, R.: Entrainment of Cold Gas into Thermal Plasma Jets, Plasma Chem. Plasma Proc., vol. 11, (4), 1991, pp. 529-543.

12. Fincke, J.R.; and Pentecost, C.G.: Laminar-to-Turbulent Transition and Entrainment in Thermal Plasma Jets, ASME Heat Transfer in Thermal and Plasma Processing, HTD vol. 161, 1991, pp. 101-106.

13. Fincke, J.R.; Swank, W.D.; and Haggard,D.C.: Entrainment and Demixing in Subsonic Argon/Helium Thermal Plasma Jets, Proc. 1993 National Thermal Spray Conf., Anaheim, CA, 7-11 June, 1993, pp. 49-54.

14. Fincke, J.R.; Swank, W.D.; and Haggard,D.C.: Plasma/Particle Interaction in Subsonic Argon/Helium Thermal Plasma Jets, Proc. 1993 National Thermal Spray Conf., Anaheim, CA, 7-11 June, 1993, pp. 25-30.

15. Spalding, D.B.: Two-Fluid models of turbulence, NASA Langley Workshop on Theoretical Approaches to Turbulence, Hampton, VA (1984).

16. Ilegbusi, O.J.; and Spalding, D.B.: A Two-Fluids Model of Turbulence and its Application to Near-Wall Flows, PCH Physico Chemical Hydrodynamics, vol. 9, (1/2), 1987, p.127.

17. Ilegbusi, O.J.; and Spalding, D.B.: Application of a Two-Fluids Model of Turbulence to Turbulent Flows in Conduits and Free Shear Layers, PCH Physico Chemical Hydrodynamics, vol. 9, (1/2), 1987, p.161.

18. Reynolds, O.: On the Extent and Action of the Heating Surface for Steam Boilers, Proc. Manchester Lib Phil Soc., vol 8, 1874.

19. Prandtl L.: Bericht uber Untersuchungen zur ausgebildeten Turbulenz, Z. angew Math. Mech. (ZAMM), vol 5, (2), 1925, pp.136-139.

20. Libby, P.A.: On the Prediction of Intermittent Turbulent Flows, J. Fluid Mech, vol. 68 (2), 1975, pp. 273-295.

21. Moss, J.B.: Simultaneous Measurements of Concentration and Velocity in an Open Pre-Mixed Flame, Comb. Sci. Tech., vol 22, 1980, pp. 115-129.

22. Bray, K.N.C.; and Libby, P.A.: Countergradient Diffusion in Pre-Mixed Turbulent Flames, AIAA J. vol 19, 1981, p.205.

23. Kollman, W.: Prediction of Intermittency Factor for Turbulent Shear Flows, AIAA J., vol. 22, 1983, pp. 486-492.

24. Ilegbusi, O.J.; and Spalding, D.B.: Prediction of Fluid Flow and Heat Transfer Characteristics of Turbulent Shear Flows with a Two-Fluid Model of Turbulence, Int. J. Heat Mass Trans., vol. 32, (4), 1989, pp. 767-773.

25. Malin, M.R.; and Spalding, D.B.: A Two-Fluid Model of Turbulence and its Application to Heated Plane Jets and Wakes, PCH Journal, vol. 5, 1984, pp.339-361.

26. Townsend, A.A.: The Structure of Turbulent Shear Flow, 2nd Edition, Cambridge University Press, 1980.

27. Rosten H.; and Spalding, D.B.: PHOENICS Beginner's Guide and User's Manual, CHAM Limited (UK) Technical Report TR/100, 1986.

28. Spalding, D.B.: Numerical Computation of MultiPhase Fluid Flow and Heat Transfer, In Recent Advances in Numerical Methods, Ed. C. Taylor and K. Morgan, 1980.

29. Spalding, D.B.: IPSA 1980 - Developments in the Procedure for Numerical Computation of Multi-Phase Flow Phenomena with Interphase Slip, Unequal Temperatures, etc., In Numerical Properties and Methodologies in Heat Transfer, Proc. 2nd Nat. Symp., Ed. T.M. Shih, Maryland, USA, 1981.

30. Spalding, D.B.: Four Lectures on the PHOENICS Computer Code, Imperial College, London, Technical Report CFD/82/5, 1982.

31. Evans, D.C.; and Tankin, R.S.: Phys. Fluids, vol. 10, 1967, p.1137.

32. Morris, J.C.; Bach,G.R.; and Yos, J.M.: Report No. ARL-64-180, Aerospace Research Laboratories, 1964.

33. Yos, J.M.: Technical Memorandum RAD-TM-63-7, Research and Advanced Development Division, AVCO Corporation, Wilmington, MA, 1983.
34. Wygnanski, I; and Fiedler, H: Some measurements in the self-preserving jet, J. Fluid Mech., vol.38, 1969 p.599.
35. Chevray, R.; and Tutu, N.K.: Intermittency and Preferential Transport of Heat in a Round Jet, J. Fluid Mech., vol. 88 (1), 1978, p.133.
36. Van der Hegge Zijnen, B.G.: Measurement of the distribution of heat and matter in a plane turbulent jet of air, Appl. Scient. Res., vol. 4, 1968, p.405.
37. Rodi,W.: A Review of Experimental Data on Free Turbulent Boundary Layers, In Studies in Convection, Theory, Measurements and Applications, Ed. B.E. Launder, Academic Press, London, 1975.
38. Davies, A.E.; Keffer, J.F.; and Baines,W.D.: Spread of a Heated Turbulent Jet, Phys. Fluids, vol. 18, (7), 1975, p.770.
39. Rodi, W.: The Prediction of Free Turbulent Boundary Layers by the use of Two-Equation Model of Turbulence, PhD. Thesis, University of London, 1972.
40. Brossa, M.; and Pfender, E.: Plasma Chem. Plasma Proc., vol. 8, 1988, p.75.

## List of Symbols

| | |
|---|---|
| D | Diameter of torch at exit |
| $E_{ij}$ | Volumetric entrainment rate of fluid j by fluid i |
| $F_{ij}$ | Volumetric inter-fluid friction |
| k | Turbulence kinetic energy |
| $l$ | Length scale |
| P | Static pressure |
| $Q_{ij}$ | Heat transfer by conduction at the interface |
| r | Volume fraction |
| $r$ | Radial coordinate |
| $r_o$ | Radius of torch at exit (D/2) |
| $r_g$ | Radial extent of computational grid |
| S | Intra-fluid source term |
| S* | Inter-fluid source term |
| $S_v$ | Shear source in radial velocity equations |
| T | Temperature |
| U | Velocity vector |
| v | Velocity component in radial direction |
| $\underline{w}$ | Velocity component in streamwise direction |
| $\overline{vT}$ | Turbulent heat flux |
| $\overline{vw}$ | Turbulent shear stress |
| y | Radial coordinate direction |
| z | Streamwise coordinate direction |
| $\delta$ | Momentum boundary layer thickness |
| $\delta_T$ | Thermal boundary layer thickness |
| $\varepsilon$ | Rate of dissipation of turbulence energy |
| $\phi$ | Generic flow variable |
| $\Gamma$ | Diffusion flux coefficient |
| $\rho$ | Fluid density |
| $\sigma$ | Prandtl number |

Table 1: Exchange Coefficients and Source Terms

| Equation | $\Gamma_i$ | $S_i$ | $S^*_i$ |
|---|---|---|---|
| Mass balance | 0 | 0 | $E_{ij}$ |
| Momentum (Radial) | $c_t k_T \tau_j |V|$ | $-\tau_i \nabla P + S_{vi}$ | $F_{ij} + U_j E_{ij}$ |
| Momentum (Axial) | $c_t k_T \tau_j |V|$ | $-\tau_i \nabla P$ | $F_{ij} + U_j E_{ij}$ |
| Energy | $c_t k_T \tau_j |V|/\sigma_T$ | 0 | $Q_{ij} + c_p T_j E_{ij}$ |

Table 2: Values of the Two-Fluid Model Constants

| Constant | Value |
|---|---|
| $c_m$ | 10.00 |
| $c_v$ | 0.30 |
| $c_d$ | 1.00 |
| $c_f$ | 0.05 |
| $c_t$ | 10.00 |
| $c_h$ | 0.05 |
| $\sigma_t$ | 1.00 |

Table 3: Principal Input Parameters

| | |
|---|---|
| Plasma Torch Diameter | 8mm |
| Maximum Plasma Temperature | 11500K |
| Maximum Plasma Velocity | 400m/s |
| Nitrogen Temperature | 300K |

Table 4: Predicted and Measured Integral Characteristics of Jets

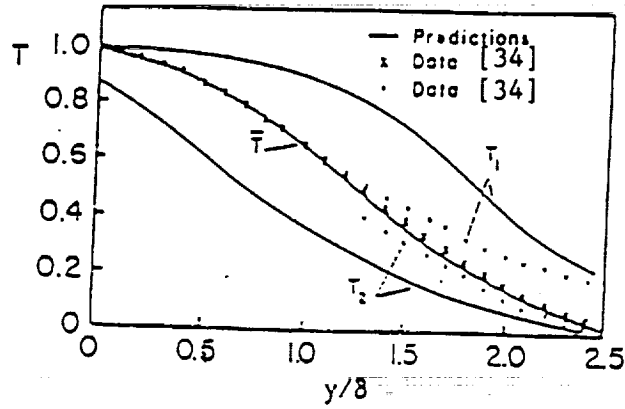| Parameter | Round Jet | | Plane Jet | |
|---|---|---|---|---|
| | Data | Prediction | Data | Prediction |
| $d\delta/dz$ | 0.086 | 0.087 | 0.110 | 0.120 |
| $d\delta_T/dz$ | 0.110 | 0.105 | 0.140 | 0.145 |
| $\overline{vw}_{max}$ | 0.019 | 0.014 | 0.024 | 0.020 |
| $\overline{vT}_{max}$ | 0.021 | 0.020 | 0.028 | 0.029 |
| $E_{max}$ | 0.051 | 0.050 | - | 0.060 |

FIGURE CAPTIONS

Fig.1    Predicted mean and fluid temperatures compared with measured
        similarity profiles of mean and conditioned data for plane jet
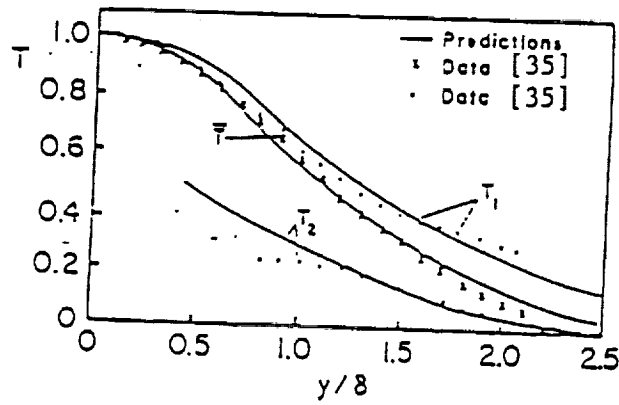
Fig.2    Predicted mean and fluid temperatures compared with measured
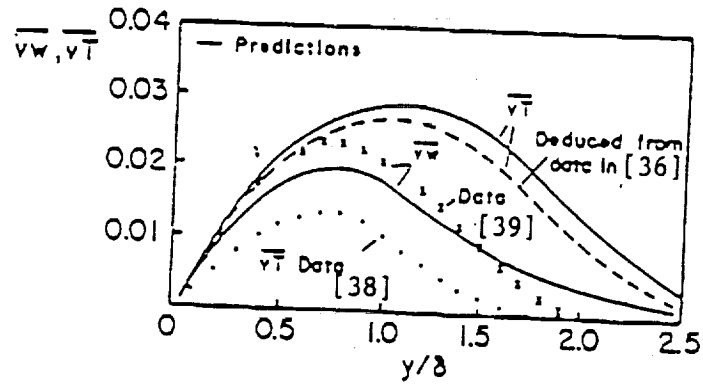        similarity profiles of mean and conditioned data for round jet

Fig.3    Predicted and measured similarity profiles of shear stress
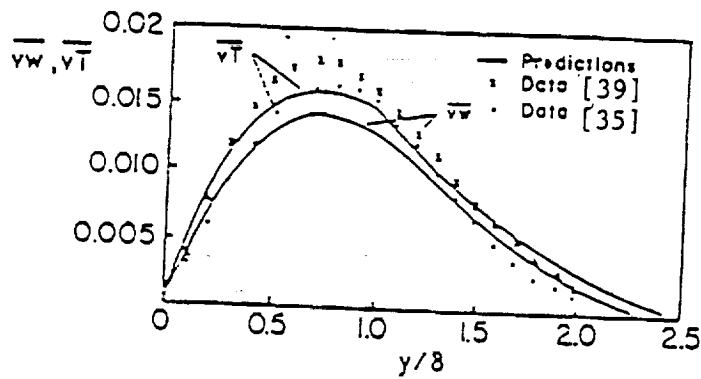        and heat flux for a plane jet

Fig.4    Predicted and measured similarity profiles of shear stress
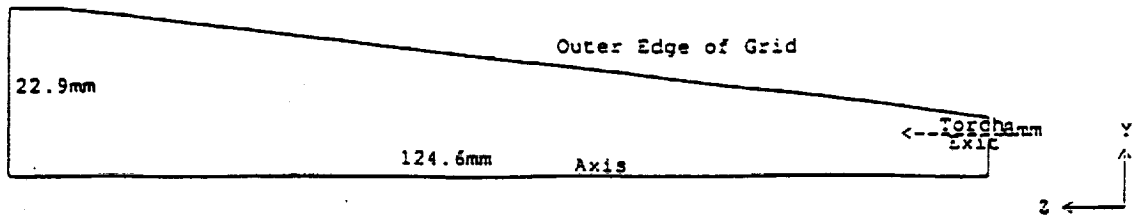        and heat flux for a round jet

Fig.5    Schematic sketch of the calculation domain employed for plasma jet
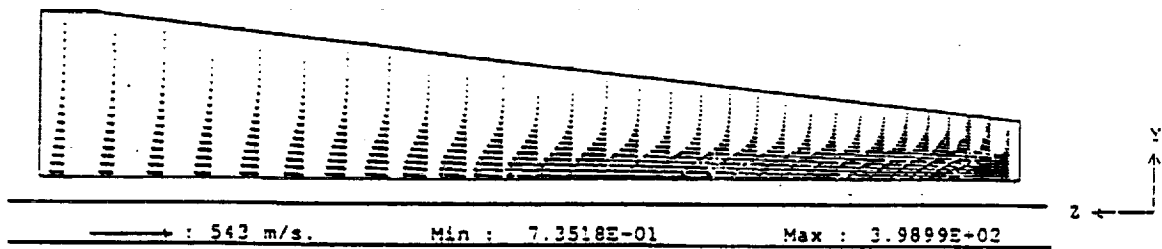
Fig.6    Velocity vectors in the plasma jet

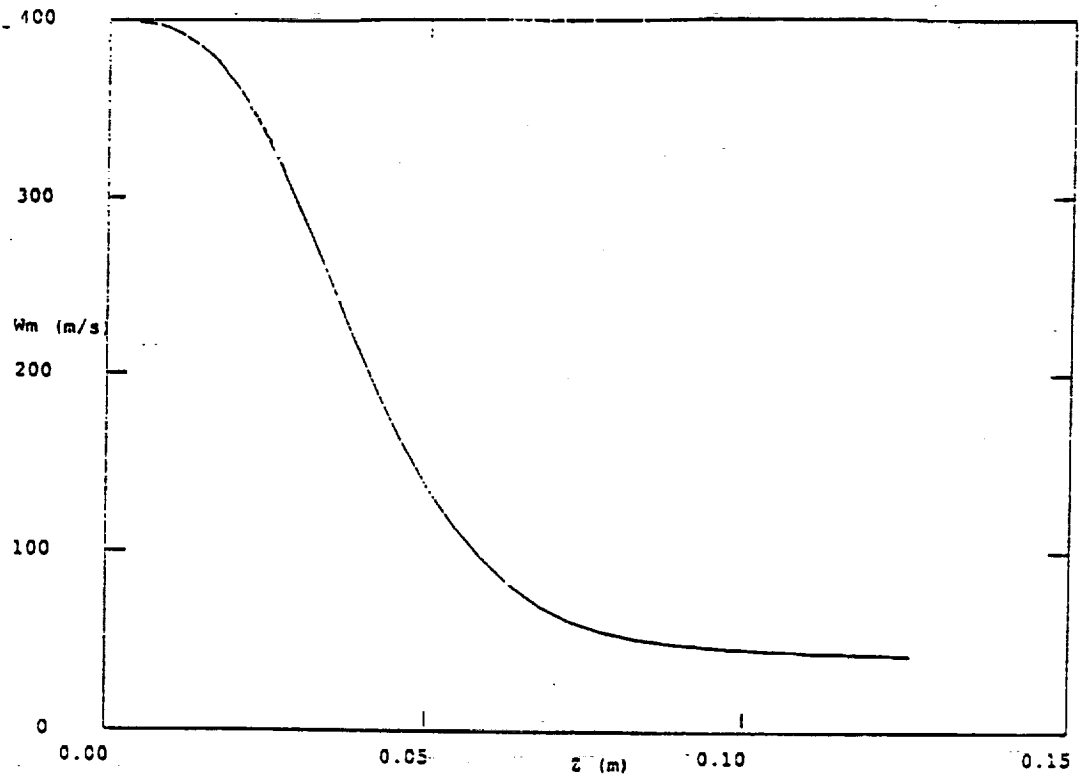Fig.7    Mean temperature profile in the plasma jet

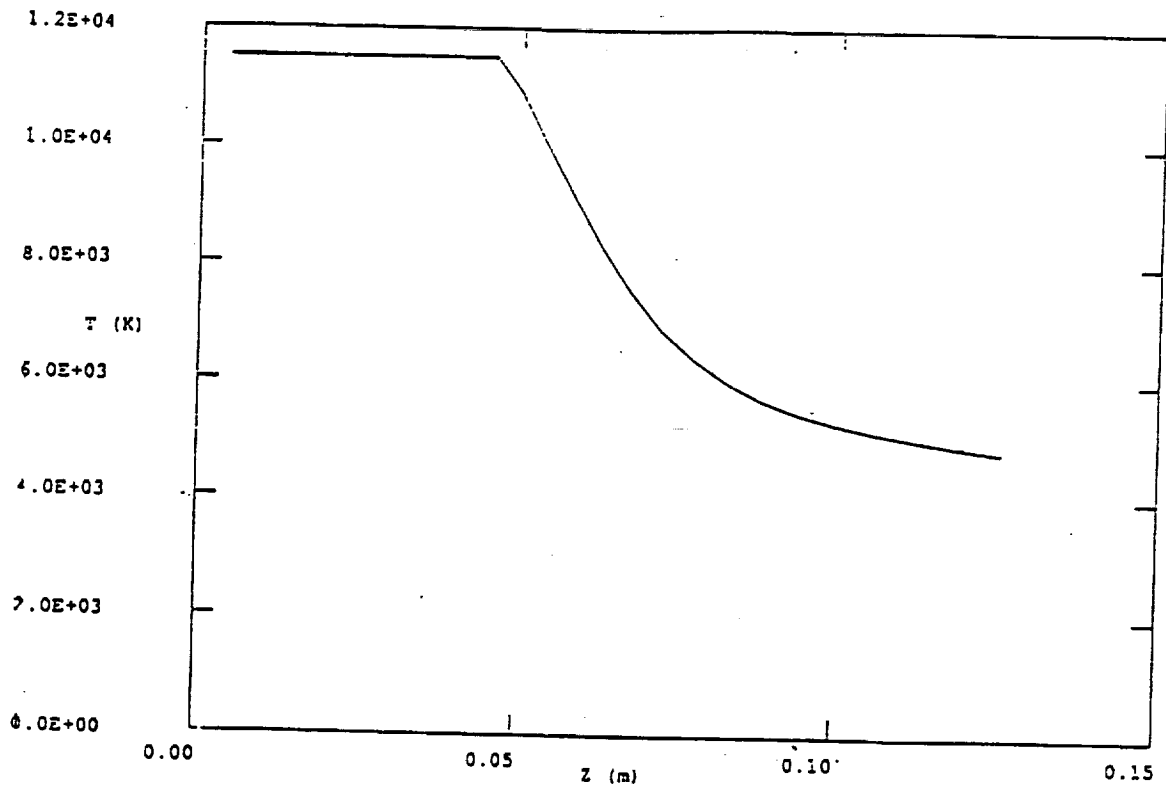Fig.8    Mean velocity decay along the jet axis

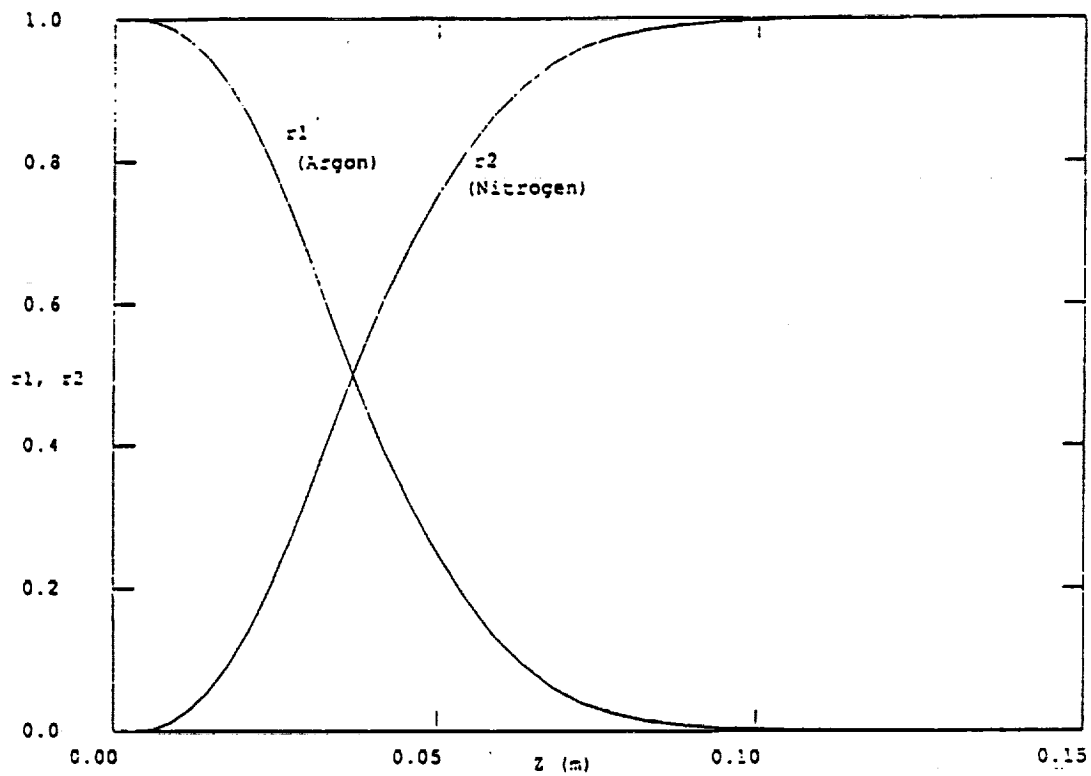Fig.9    Mean temperature decay along the jet axis

Fig.10   Volume fractions of Argon and Nitrogen along jet axis

Fig.11   Profile of volumetric entrainment rate in the plasma jet
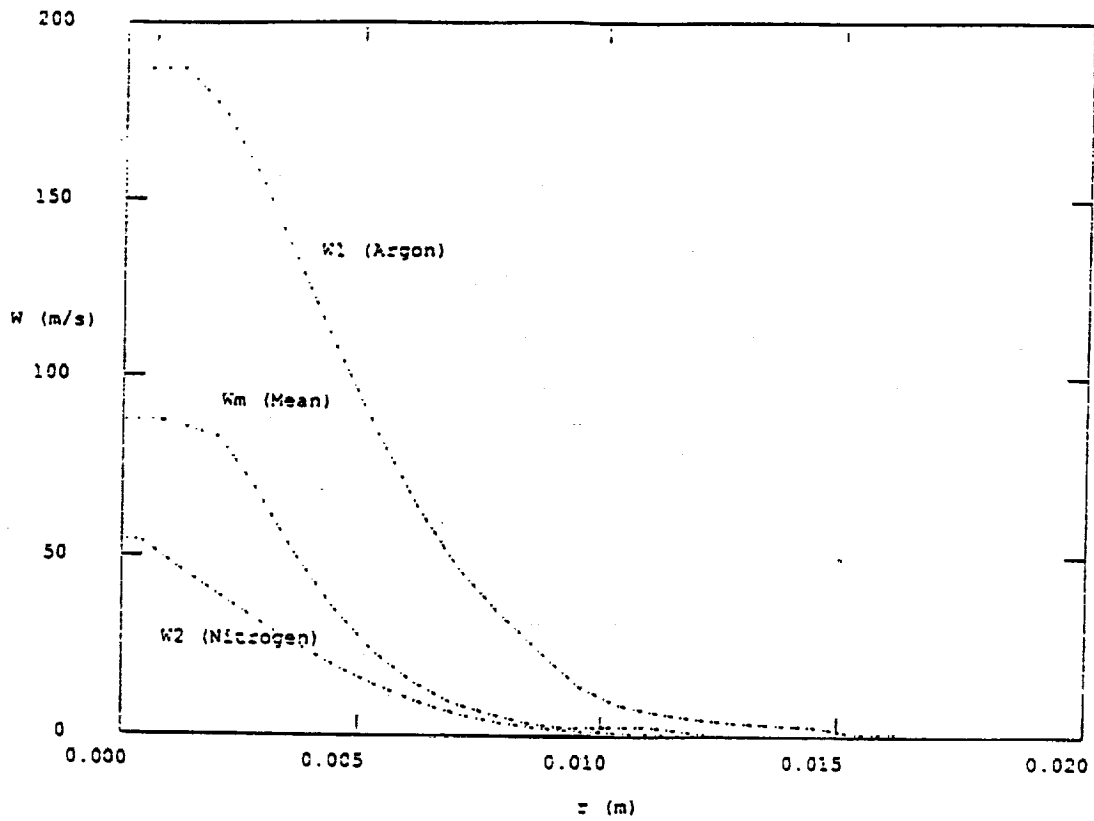
Fig.12   Predicted radial variation of velocities of Argon and Nitrogen at $z/D=5$
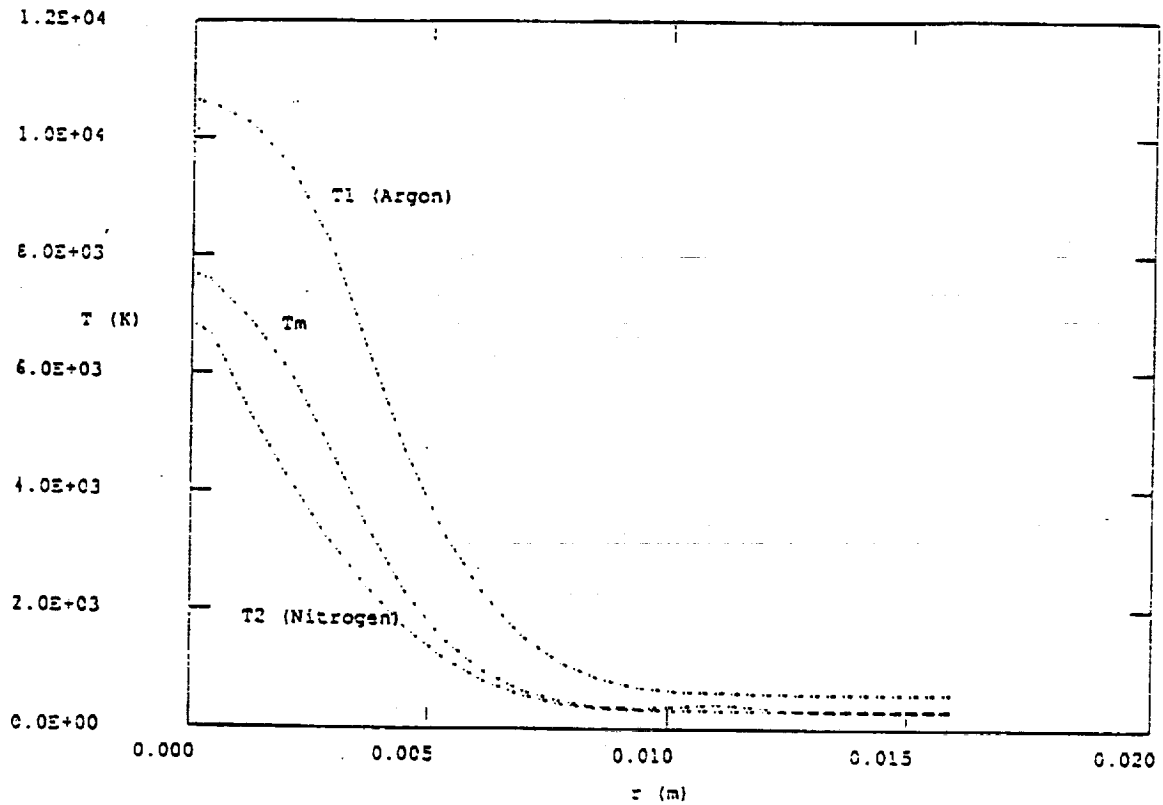
Fig.13   Predicted radial variation of temperatures of Argon and Nitrogen at $z/D=5$

Fig.14   Profile of Argon temperature in the jet

Fig.15   Profile of Nitrogen temperature in the jet

Fig.16   Radial variation of Argon temperature at $z/D=3,5$ and 8.

Fig.17   Radial variation of Nitrogen temperature at $z/D=3,5$ and 8

Fig.18.  Predicted centerline profile of mean temperature compared
        with the experimental data of ref. 40.

Fig.19.  Predicted radial profile of mean temperature at $z=20mm$ compared
        with the experimental data of ref. 40.

319

Fig.1 Predicted mean and fluid temperatures compared with measured similarity profiles of mean and conditioned data for plane jet



Fig.2 Predicted mean and fluid temperatures compared with measured similarity profiles of mean and conditioned data for round jet

Fig.3    Predicted and measured similarity profiles of shear stress
and heat flux for a plane jet



Fig.4    Predicted and measured similarity profiles of shear stress
and heat flux for a round jet

Fig.5  Schematic sketch of the calculation domain employed for plasma jet



Fig.6  Velocity vectors in the plasma jet



Fig.7  Mean temperature profile in the plasma jet

Fig.8 Mean velocity decay along the jet axis



Fig.9 Mean temperature decay along the jet axis

Fig.10 Volume fractions of Argon and Nitrogen along jet axis



Fig.11 Profile of volumetric entrainment rate in the plasma jet

324

Fig.12 Predicted radial variation of velocities of Argon and Nitrogen at z/D=5



Fig.13 Predicted radial variation of temperatures of Argon and Nitrogen at z/D=5

325

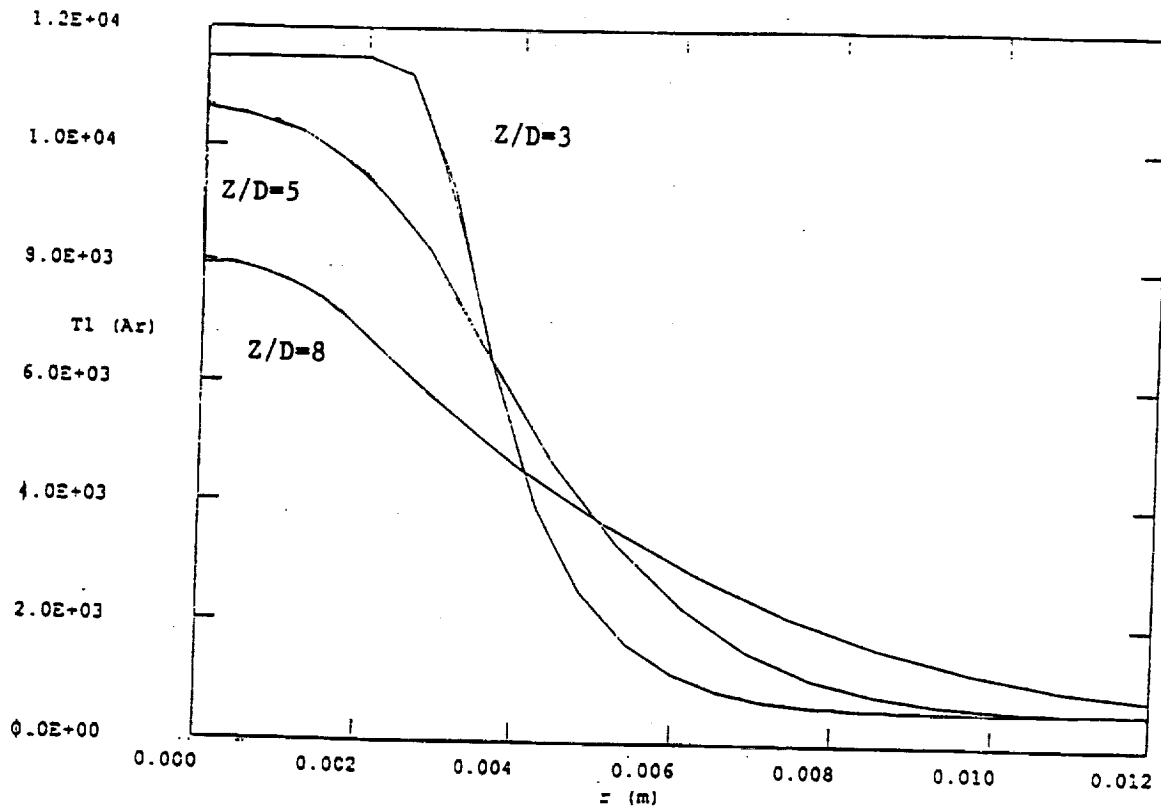Fig.14 Profile of Argon temperature in the jet



Fig.15 Profile of Nitrogen temperature in the jet

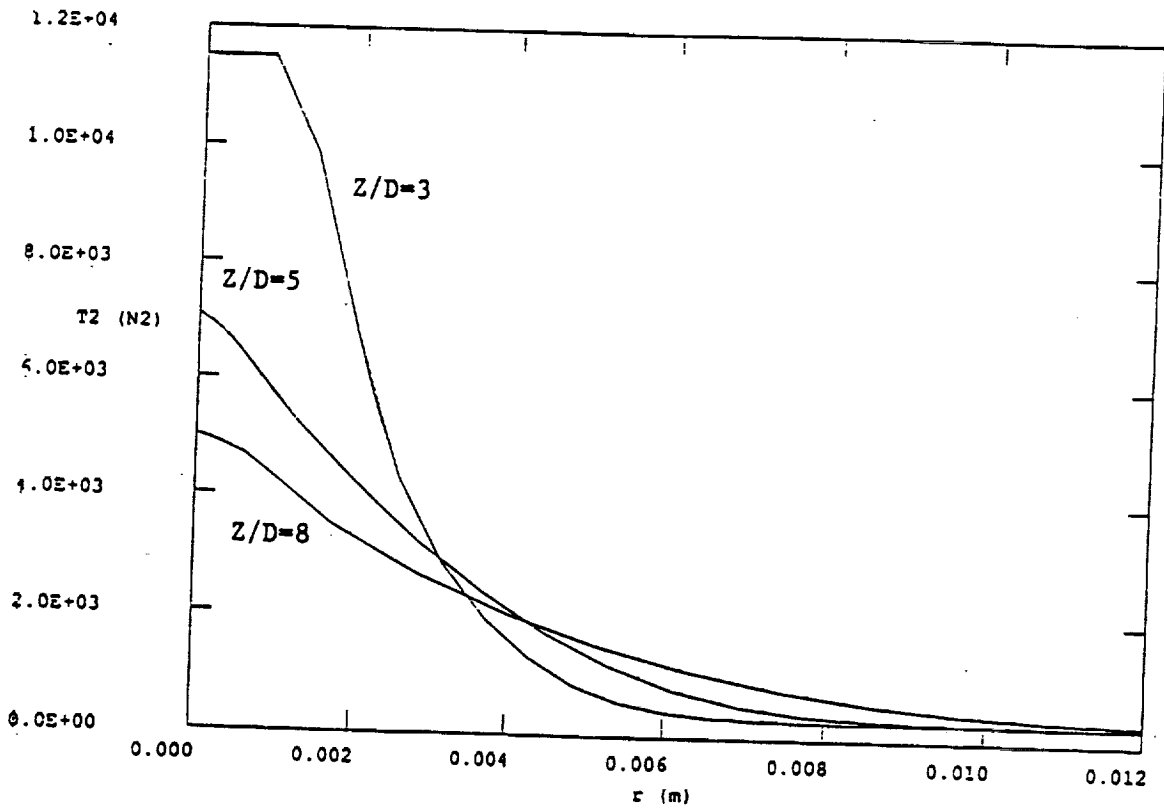Fig.16 Radial variation of Argon temperature at z/D=3,5 and 8.



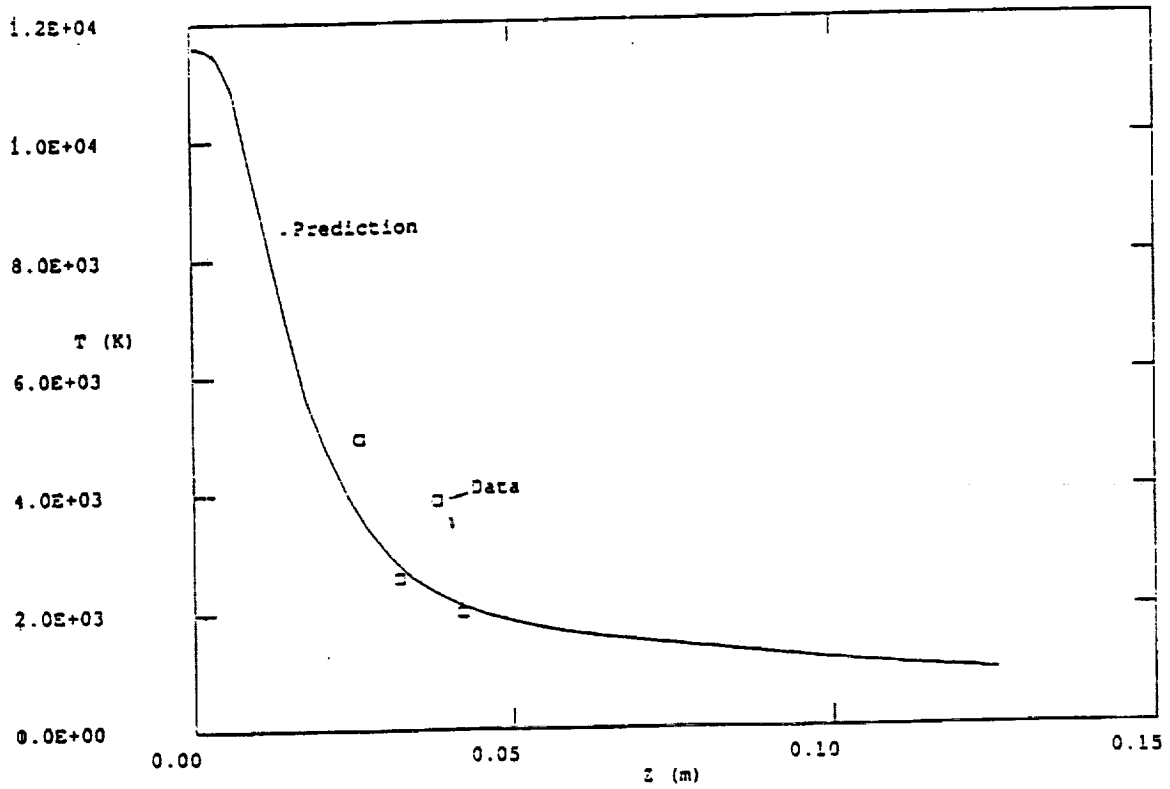Fig.17 Radial variation of Nitrogen temperature at z/D=3,5 and 8

Fig.18. Predicted centerline profile of mean temperature compared
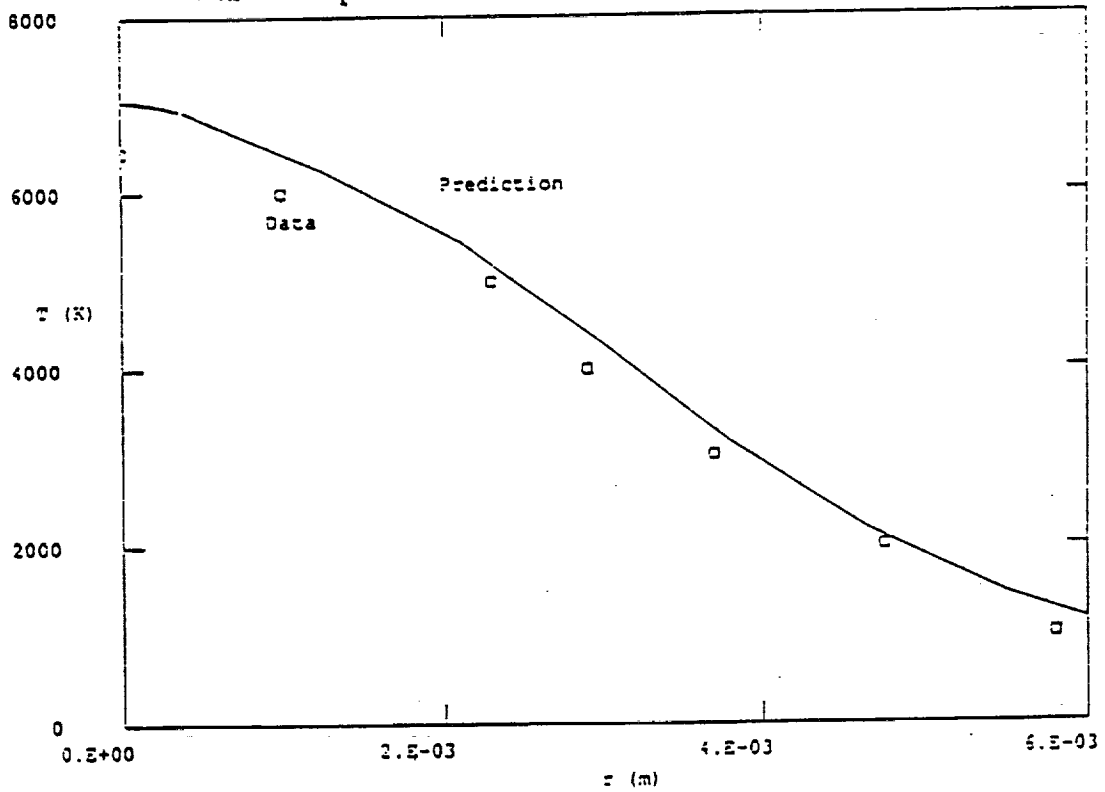with the experimental data of ref. 40.



Fig.19. Predicted radial profile of mean temperature at z=20mm compared
with the experimental data of ref. 40.

328